



## Effective reinforcement of plasticized starch by the incorporation of graphene, graphene oxide and reduced graphene oxide

Kizkitza González <sup>a,b</sup>, Izaskun Larraza <sup>a</sup>, Loli Martin <sup>c</sup>, Arantxa Eceiza <sup>a</sup>, Nagore Gabilondo <sup>a,\*</sup>

<sup>a</sup> Department of Chemical and Environmental Engineering, 'Materials+Technologies' Group, Engineering College of Gipuzkoa, University of the Basque Country (UPV/EHU), Plaza Europa 1, 20018 Donostia-San Sebastián, Spain

<sup>b</sup> Department of Graphical Expression and Project Management, Engineering College of Gipuzkoa, University of the Basque Country (UPV/EHU), Plaza Europa 1, 20018 Donostia-San Sebastián, Spain

<sup>c</sup> Macrobehaviour-Mesostructure-Nanotechnology SGiker Service, Faculty of Engineering of Gipuzkoa, University of the Basque Country (UPV/EHU), Plaza Europa 1, Donostia-San Sebastián 20018, Spain



### ARTICLE INFO

#### Keywords:

Plasticized starch  
Graphene oxide  
Electrical response

### ABSTRACT

Plasticized starch (PLS) nanocomposite films using glycerol and reinforced with graphene (G) and graphene oxide (GO) were prepared by solvent casting procedure. On one hand, the influence of adding different G contents into the PLS matrix was analyzed. In order to improve the stability of G nanoflakes in water, *Salvia* extracts were added as surfactants. The resulting nanocomposites presented improved mechanical properties. A maximum increase of 287 % in Young's modulus and 57 % in tensile strength was achieved for nanocomposites with 5 wt% of G. However, it seemed that *Salvia* acted as co-plasticizer for the PLS. Moreover, the addition of the highest G content led to an improvement of the electrical conductivity close to  $5 \times 10^{-6}$  S/m compared to the matrix.

On the other hand, GO was also incorporated as nanofiller to prepare nanocomposites. Thus, the effect of increasing the GO content in the final behavior of the PLS nanocomposites was evaluated. The characterization of GO containing PLS nanocomposites showed that strong starch/GO interactions and a good dispersion of the nanofiller were achieved. Moreover, the acidic treatment applied for the reduction of the GO was found to be effective, since the electrical conductivity was 150 times bigger than its G containing counterpart.

### 1. Introduction

Nowadays, multidisciplinary researchers are focused on the development of new environmentally friendly and biopolymer-based materials with competitive and specific properties, such as electrical conductivity [1–3]. Biopolymers are usually non-conductive macromolecules, but adding conductive inorganic nanofillers (carbon nanotubes, multi-walled carbon nanotubes, graphite, graphene) into the biopolymer matrix, the electrical conductivity could be improved [4–8].

In this context, polysaccharides such as cellulose, lignin, chitosan or starch become the perfect alternative to conventional electrically conductive polymers [1]. Among the above mentioned polysaccharides, starch is a promising natural polymer, due to its availability, versatility, biodegradability, low cost as well as its non-toxic properties [9–11]. However, starch shows some disadvantages such as its hydrophilicity and poor mechanical and electrical properties [12,13].

To overcome these drawbacks, PLS matrices could be reinforced adding carbonaceous nanoparticles such as graphene (G), graphene oxide (GO) or reduced graphene oxide (rGO) [12]. G is the allotropic form of carbon where a single layer of  $sp^2$  bonded carbon atoms are packed in a two dimensional honeycomb lattice [14,15]. G presents unique optical, mechanical and electrical properties, as well as large specific surface area [16,17].

Unfortunately, G presents poor dispersibility in polar solvents as is water [14,16]. In fact, in order to facilitate the dispersion of G in aqueous media, the use of different types of surfactants has been proposed in literature [18,19]. Among them, those containing phenolic moieties have been reported to be highly "graphene-philic" due to the formation of  $\pi$ - $\pi$  interactions with G and, hence, increasing the stability of the dispersion [20]. Indeed, it was demonstrated that natural plant extracts, such as *Salvia officinalis L.*, can act as dispersion stabilizers due to the presence of polyphenolic groups on its chemical structure [21].

\* Corresponding author at: University of the Basque Country, Plaza Europa, 20018 San Sebastián, Spain.  
E-mail address: [nagore.gabilondo@ehu.eus](mailto:nagore.gabilondo@ehu.eus) (N. Gabilondo).

Besides to the addition of surfactants, the oxidation and subsequent reduction of GO have been also suggested as a strategy for the incorporation of G in aqueous systems. Therefore, GO and rGO are commonly preferred as nanofiller in numerous cases to improve the mechanical and electrical properties of several materials [22–25] due to its unique physicochemical properties [26]. The obtained GO nanoflakes present the G skeleton while it contains oxygen containing functional groups (i.e. hydroxyl, epoxide, carbonyl and/or carboxyl groups) in the basal plane and the flake edges [27,28]. These functionalities make GO more hydrophilic [29], facilitating its dispersion in polar solvents and water, as well as the formation of strong filler/matrix hydrogen bonding interactions [28,30] and thus, leading to a better dispersion of the nanofiller [14]. In the case of starch-based materials reinforced with GO, strong hydrogen bonding could be expected between the hydroxyl groups of starch and the aforementioned functional groups of GO [31,32].

However, GO presents the disadvantage of being electrically non-conductive due to both the chemical reactive groups and the presence of defects on its structure [33]. For this reason, GO is usually chemically reduced. Hence, the  $sp^2$  hybridized structure is partially restored, thus the resulting rGO presents excellent mechanical properties and electrical conductivity [34–37]. The GO is not usually completely reduced, and, consequently, the residual functional oxygen groups that remains in the surface of rGO allow the formation of polymer/rGO interactions [38–40]. The reduction reaction could be carried out using hydrazine, sodium hydrosulphite, sodium borohydride, glucose or hydroquinone as reducing agents, among others [33,35]. Nevertheless, in the last years, vitamin C (ascorbic acid) has been proposed as an eco-friendly effective reducing agent for the GO [33,41].

The aim of this work was the development of starch-based films with improved mechanical properties and supplied with electrical conductivity by the incorporation of graphite-derived nanoentities. For this, two different nanocomposite preparation routes have been proposed. On the one hand, it was hypothesized that the incorporation of G nanoflakes, stabilized with *Salvia* extracts, should improve the mechanical and electrical behavior of the PLS films, due to its shown great specific properties. On the other hand, the use of GO as reinforcement was considered, willing to benefit from its functional groups able to form strong polymer/filler interactions leading to highly reinforced materials. Moreover, the subsequent reduction to rGO could lead to enhanced electrical behavior since the  $sp^2$  hybridized structure could be restored.

## 2. Experimental

### 2.1. Materials

Normal maize starch composed of 73 % amylopectin and 27 % amylose (purchased from Sigma-Aldrich, USA), and glycerol (99 %, from Panreac, Spain) were employed to prepare the PLS films and nanocomposite films. Graphite flakes provided by Sigma-Aldrich (USA) were used to obtain G and GO. Besides, for the obtainment of G and GO and the reduction to rGO the following reactants were also employed: N-methyl pyrrolidone (NMP, 97 %, from Sigma-Aldrich, USA), sodium nitrate ( $NaNO_3$ , 99 %), sulfuric acid ( $H_2SO_4$ , 96 %), potassium permanganate ( $KMnO_4$ , 99 %), hydrogen peroxide ( $H_2O_2$ , 30 % w/v), hydrochloric acid (HCl, 37 %) and ascorbic (Panreac, Spain). For obtaining the plant extracts used as emulsifier of G, *Salvia officinalis* L. was employed as dry material purchased in an herbalist. All reagents were employed as received. Distilled water was used as solvent.

### 2.2. Preparation of graphene nanoflakes

The preparation of G was performed as described in literature [42,43]. 20 g of graphite were sonicated in 1500 mL of NMP for 100 h. In order to keep the smaller fraction, the obtained dispersion was centrifuged at 4000 rpm for 45 min and the supernatant was filtered

(Polyamide filters, Sartorius, pore size 0.2  $\mu$ m), washed with acetone and dried for 48 h at room temperature. The success of the procedure was demonstrated by the characterization of G in our previous work [42].

### 2.3. Obtainment of *Salvia* extracts

The preparation of *Salvia* extracts was carried out by infusion method according to the protocol described in a previous work [18]. Briefly, 20 g of *Salvia officinalis* L. were boiled with 800 mL of distilled water for 5 min. After that, the obtained suspension was filtered and freeze-dried.

### 2.4. Preparation of graphene oxide nanoflakes

The GO nanoflakes were obtained following the protocol defined by Larraza et al. [42], which consists in the Hummers' method with slight differences. 1 g of graphite was mixed and stirred with 0.5 g of  $NaNO_3$  and 23 mL of  $H_2SO_4$  (96 % purity) for 30 min at 0 °C. After that, 3 g of  $KMnO_4$  were added and the resulting dispersion was maintained in continuous magnetic stirring during 2 h at 0 °C. Then, the mixture was heated for 30 min at 35 °C. Next, 46 mL of distilled water were added drop by drop, heated at 98 °C and maintained during 30 min. Finally, 10 mL of  $H_2O_2$  (30 % purity) were added and then the reaction was cool down, 150 mL of distilled water were added. The supernatant of the mixture was discarded, and the resulting sediment was washed by centrifugation with a 5 % HCl aqueous solution (4500 rpm, 20 min, 5 times) and distilled water (4500 rpm, 20 min, until pH = 7). The sediment was filtered (Polyamide filters, Sartorius, pore size 0.2  $\mu$ m), centrifuged (4000 rpm, 3 h) and dried. The obtained GO nanoentities were already previously characterized [42].

### 2.5. Preparation of PLS based nanocomposite films

The nanocomposites containing G and GO were prepared by solvent casting (Fig. 1). 3.58 g of normal maize starch and 1.93 g of glycerol were mixed with 55 mL of distilled water. In addition, the desired amount of carbonaceous nanoparticles (0, 1, 2.5 and 5 wt% of G or GO) previously dispersed by ultrasonication was incorporated (5 mg of carbonaceous nanoparticle  $mL^{-1}$  of distilled water). For the dispersion of G nanoflakes 2.5 mg of *Salvia* extracts  $mL^{-1}$  distilled water were added as stabilizer. The mixture was gelatinized at 90 °C continuous stirring until viscosity increased (30 min). The resulting viscous gel was homogenized using a dispersing system (POLYTRON® PT 2500 E) during 3 min at 15,000 rpm. Finally, the material was spread into a glass petri dish and dried at 45 °C for 3.5 h.

A glycerol content of 35 wt% was used for all samples, i.e. relative to the starch plus plasticizer mixture weight. The nanofiller and *Salvia* extract contents were relative to the starch plus glycerol weight. All the samples were stored at a relative humidity (RH) of 43 % ( $K_2CO_3$  saturated solution) for two weeks before characterization, since the RH affects the properties of starch films, and willing to avoid the effect of external parameters. The conditioning time and RH were selected considering previous works [13,44].

Samples were called as PLS plus the carbonaceous nanoparticle content, indicating GE or GO if G and extracts or GO was used (PLS - wt% GE or PLS - wt% GO).

### 2.6. Reduction of graphene oxide

The rGO was obtained using ascorbic acid as reducing agent [45]. The nanocomposites containing GO were submerged in a solution of 30 g of ascorbic acid  $L^{-1}$  of distilled  $H_2O$  at 95 °C for 2 h. After that, in order to remove the excess of ascorbic acid, the films were washed several times with distilled water. Finally, the films were dried at room temperature for 24 h. Samples were named as PLS plus the rGO content (PLS - wt% rGO).

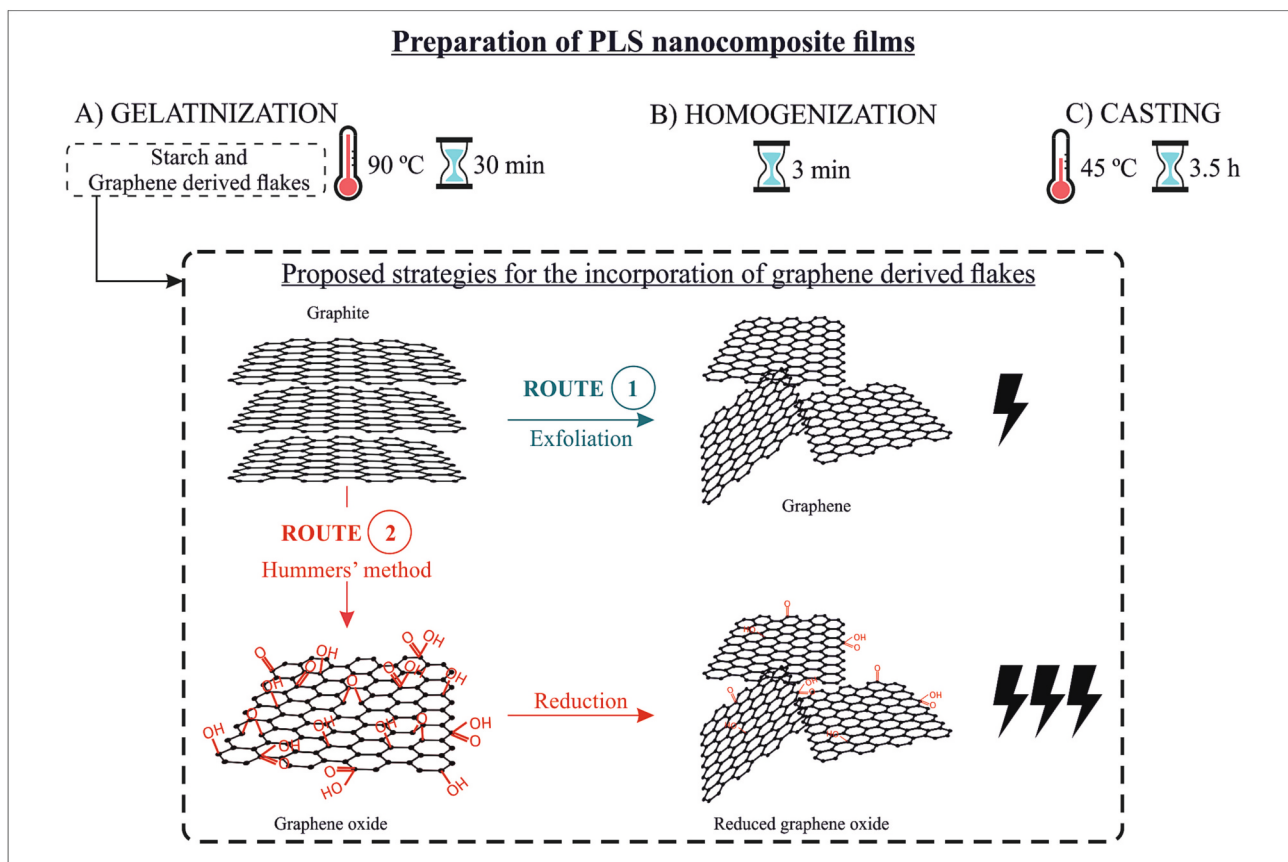


**Fig. 1.** Followed methodology and proposed routes for the preparation of PLS nanocomposite films.

## 2.7. Characterization methods

The characteristic functional groups of the starch matrix and the resulting nanocomposites were analyzed by Fourier transform infrared spectroscopy (FTIR), using a Nicolet Nexus spectrophotometer (Thermo Fisher Scientific, USA). Measurements were recorded in the range from 4000 cm<sup>-1</sup> to 650 cm<sup>-1</sup> in attenuated total reflection (ATR) mode, with a 4 cm<sup>-1</sup> resolution and 32 scans. The spectra were recorded with a Specac MKII Golden Gate accessory equipped with a diamond crystal at a nominal incident angle of 45° and ZnSe lens.

X-ray diffraction (XRD) measurements were performed using a Philips Xpert Pro automatic diffractometer (Malvern Panalytical, UK) operating at 40 kV and 40 mA, in θ - θ configuration, a secondary monochromator with Cu-Kα radiation ( $\lambda = 1.5418 \text{ \AA}$ ) and a PIXcel solid state detector (active length in 2θ = 3.347°). Scattered radiation was detected in the angular range 2θ = 2–40° (step size 0.026 and time per step 80 s) at room temperature. The interlayer distance was calculated following the Bragg's law [46]:

$$n\lambda = 2dsin\theta \quad (1)$$

where  $n$  is a whole number (in our case 1),  $\lambda$  is the incident radiation wavelength (0.154 nm),  $d$  is the shortest distance between successive identical planes in the crystal which is associated to the interlayer separation and  $\theta$  is the angle of incidence of the primary rays on the plane.

Static contact angle measurements of nanocomposite films were performed using a Surface Electro Optics (SEO) Phoenix Series P-300 equipment (Malasya) with a needle-in-drop technique. The contact angle measurements were carried out at room temperature, with a drop volume of 3.0 μL and using ethylene glycol as solvent. Five samples of each system were tested and an average value was calculated.

The viscoelastic behavior of nanocomposite films was analyzed by

dynamic mechanical analysis (DMA), using an Eplexor 100 N instrument from Gabo Qualimeter (Germany) registering the storage modulus ( $E'$ ), the loss modulus ( $E''$ ) and the  $\tan \delta = E''/E'$ . Measurements were performed at 1 Hz and with a heating rate of 2 °C min<sup>-1</sup>, working in tensile mode from -100 °C to 0 °C and an initial strain of 0.5 %. The samples were cut as rectangular strips (25.0 × 3.0 × 0.2 mm<sup>3</sup>). Three specimens of each system were measured and averaged.

Tensile tests were performed using an Instron 5967 equipment (Instron, USA), provided with a load cell of 500 N and pneumatic grips to hold the samples. Samples were cut into dumbbell shaped specimens with a testing section of 0.2 mm in thickness and 5 mm in width. Tests were performed at a crosshead rate of 5 mm min<sup>-1</sup>, at room temperature and with a distance between clamps of 15 mm. Tensile modulus ( $E$ ), stress at yield ( $\sigma_y$ ), stress at break ( $\sigma_b$ ) and elongation at break ( $\epsilon_b$ ) were determined from stress-strain curves of five specimens of each system.

The electrical response was analyzed by a Keithley 4200-SCS equipment (Keithley Instruments, USA) for semiconductor analysis. Two-point measurements were carried out, performing 0–5 V linear scans, with a 0.01 V step and a compliance of 0.1 A. Electrical resistance ( $R$ ) values were calculated as the slope measured from intensity vs. voltage curves (as shown in Fig. S1), resistivity ( $\rho$ ) and conductivity ( $\Theta$ ) values were calculated using Eqs. (2) and (3). Five specimens of every system were analyzed and averaged.

$$\rho = R \frac{A}{L} \quad (2)$$

where  $R$  is the resistance, and  $A$  and  $L$  are the area and length of the tested sample, respectively.

$$\Theta = \frac{1}{\rho} \quad (3)$$

Transmission electron microscopy (TEM) images were recorded on a FEI Titan Cubed G2 60–300 microscope (Thermofisher Scientific, USA), equipped with a Schottky X-FEG field emission electron gun, monochromator and CEOS GmbH spherical aberration (Cs) corrector on the image side. The microscope was operated at 80 kV. The third-order spherical aberration (Cs) was tuned to  $-10 \mu\text{m}$ . Images were obtained for an underfocus of  $-8 \text{ nm}$  and were recorded on a CCD camera (2kx2k, Gatan UltraScan 1000), using exposition times of 1 s per image.

For TEM analysis, aqueous suspension mgs of G or Go ( $5 \text{ mg mL}^{-1}$ ) were prepared by ultrasonication (with on/off periods of 4 s and 2 s). In the case of G, *Salvia* extract was also added as stabilizer. Then, a drop of the sonicated suspension was placed in a TEM copper grid (300 Mesh) covered by a holey carbon film and dried under vacuum.

The electrical conductivity properties of the nanocomposite films were also analyzed by electrostatic force microscopy (EFM). Measurements were performed in a Dimension ICON scanning probe microscope (Bruker, USA), operating at lift mode ( $100 \text{ nm}$ ) under ambient conditions and equipped with Pt/Ir coated tips ( $75 \text{ kHz}$  resonant frequency). To analyze the distribution of the electrostatic field gradient on the sample surface, bias voltages from 0 to 10 V were applied to the cantilever/tip system. Conductive and insulating parts of the sample can be distinguished since charged areas are observed as bright zones in the EFM phase images. For each system, a sample size of  $2 \times 2 \text{ mm}$  was cut and stuck to an AFM stainless steel specimen disk.

Scanning electron microscopy (SEM) images were recorded in order to analyze the morphology of cross section surfaces of nanocomposite films. Images were obtained using a Field Emission Gun Scanning Electron Microscope (FEG-SEM) Hitachi S-4800 N (Japan) with an operation voltage of 5 kV. Specimens were coated with gold provide conductivity prior to the microscopy observation.

Quantitative experimental data is presented as mean  $\pm$  SD. In order to consider statistical relevance of the contact angle measurements as well as mechanical and electrical analysis results, one way ANOVA was carried out with OriginPro8 (Origin Lab), using the Turkey's test at a significant level of  $p < 0.05$ .

### 3. Results and discussion

#### 3.1. Effect of G content on PLS nanocomposite films

The aim of the present work was the obtaining of electrically conductive starch-based materials with enhanced mechanical properties. The first proposal to achieve this objective was the preparation of PLS nanocomposite films adding G nanoflakes into the starch-based gelatinized matrix with glycerol. In order to improve the poor

dispersibility of G in water, natural *Salvia* extracts were used as dispersion stabilizer since they present high content of polyphenolic groups. It was expected that the final properties of the material would be dependent of the G and extract content. Thus, the nanocomposites were prepared using different G and *Salvia* extracts contents (1, 2.5 and 5 wt %).

FTIR measurements were carried out to analyze the chemical structure of PLS films and obtained nanocomposites reinforced with G nanoflakes. The obtained FTIR spectra of *Salvia* extracts, PLS films and resulting nanocomposites are shown in Fig. 2.

As observed in the spectra, the unfilled PLS matrix showed the stretching band of hydrogen bonded -OH groups at  $3280 \text{ cm}^{-1}$ , whereas the -OH bending appeared at  $1650 \text{ cm}^{-1}$  [47,48]. The C—H stretching band related to methylene (-CH<sub>2</sub>) groups was centered at  $2927 \text{ cm}^{-1}$  [47,48]. In addition, in the fingerprint region of starch the following peaks were observed: the stretching vibration band of C—O bonds in C—O—H groups at  $1150 \text{ cm}^{-1}$  and the stretching vibration bands of C—O in C—O—C groups located at  $1077 \text{ cm}^{-1}$  and  $997 \text{ cm}^{-1}$  [49].

Regarding the spectra of reinforced nanocomposite films, only slight differences could be observed compared to the unfilled matrix. As it could be seen, the addition of G and *Salvia* extracts resulted in the widening and shifting to lower wavenumber value of the band associated with -OH bending. This effect could be related to the contribution of hydrophilic *Salvia* extracts that showed an intense band related with -OH bending. In addition, the small band at  $1575 \text{ cm}^{-1}$  would be related to the double bonds (C=C) of the phenolic groups from *Salvia* [50] and the aromatic structure of G ring [51].

XRD measurements were carried out in order to analyze the crystalline structure of the nanocomposites. Fig. 3 presents the XRD pattern of unfilled PLS matrix and nanocomposites obtained with G nanoflakes.

As it could be appreciated, the A-type polymorphism pattern of the native normal maize starch was replaced by a typical broad peak close to  $2\theta = 19.8^\circ$  in the case of the amorphous PLS matrix, indicating that the gelatinization occurred successfully [52]. However, all nanocomposites showed a new peak associated with G at  $2\theta = 26.5^\circ$  related to the (002) plane of the hexagonal structure of pure graphite [42]. As expected, the intensity of the mentioned new peak increased as the G content increased, indicating that the crystalline structure of G was not affected by the gelatinization and drying procedures.

Contact angle measurements were carried out in order to characterize the hydrophobicity of the nanocomposite films. As it could be observed in Table 1, the unfilled PLS matrix showed a low contact value ( $24.6^\circ$ ) due to the hydrophilic character of starch [53]. However, the incorporation of graphite to the material resulted in a significant alteration of this property for all contents of G. Upon the addition of a 1

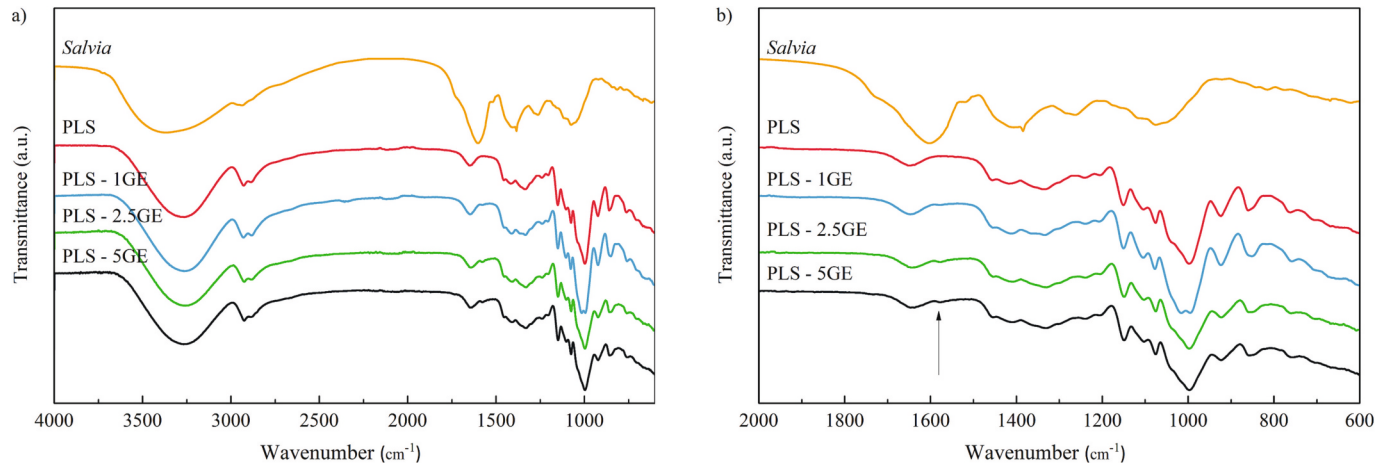


**Fig. 2.** FTIR spectra of *Salvia* extracts and PLS nanocomposite films reinforced with G in the range of a)  $4000\text{--}600 \text{ cm}^{-1}$  and b) a magnification in the range of  $2000\text{--}600 \text{ cm}^{-1}$ .

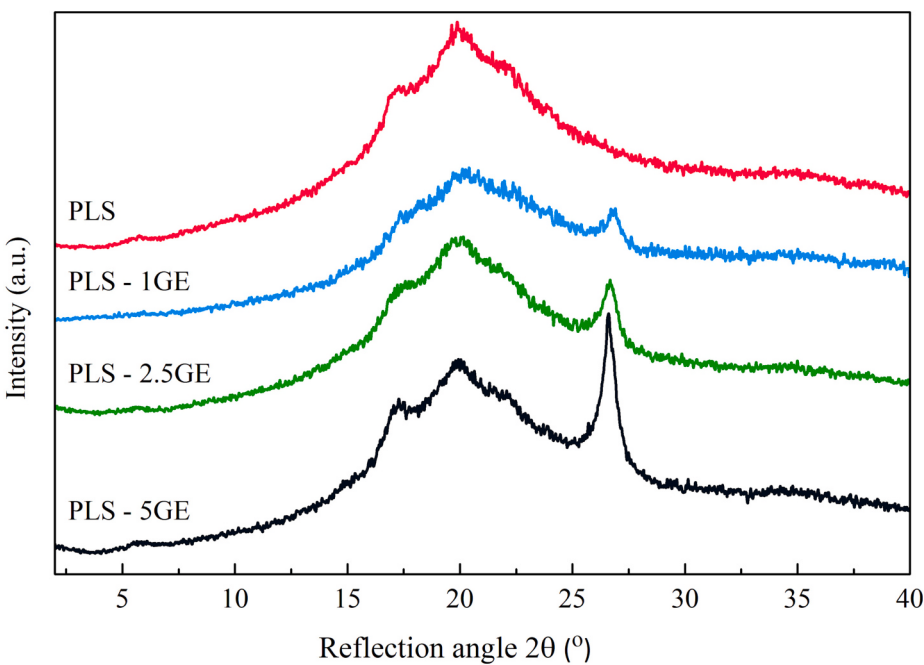


**Fig. 3.** XRD patterns of PLS nanocomposite films reinforced with G.

**Table 1**

Contact angle measurements and mechanical properties of PLS – GE nanocomposite films. Values analyzed using one-way ANOVA with Tukey's test, \* indicates statistical differences compared to the matrix, where  $p < 0.05$ .

Sample	Contact angle (°)	Young's modulus (MPa)	Tensile strength (MPa)	Strain at break (%)
PLS	$24.6 \pm 0.3$	$7.9 \pm 0.9$	$1.4 \pm 0.1$	$57.9 \pm 0.5$
PLS – 1GE	$37.2 \pm 1.9 *$	$8.1 \pm 0.1$	$1.5 \pm 0.2$	$43.6 \pm 2.7 *$
PLS – 2.5GE	$35.1 \pm 4.8 *$	$13.6 \pm 0.6 *$	$1.5 \pm 0.3$	$43.9 \pm 4.6 *$
PLS – 5GE	$35.6 \pm 2.8 *$	$30.6 \pm 2.3 *$	$2.2 \pm 0.1 *$	$41.3 \pm 2.0 *$

wt% of G, the contact angle increased up to  $37.2^\circ$ . The incorporation of higher contents of G resulted in a slight decrease of the contact angle values. Although it could be expected that the addition of G could decrease the wettability due to its hydrophobic character (as observed by FTIR), the presence of hydroxyl groups in the *Salvia* extracts, used to disperse and stabilize the hydrophobic G in the starch matrix, contributed to counteract slightly the effect of G.

The viscoelastic behavior of PLS nanocomposites reinforced with G was studied by DMA analysis. The evolution of the normalized storage modulus ( $E'/E'_g$ ) (where  $E'_g$  corresponds to the experimental storage modulus at  $-100^\circ\text{C}$ ) and  $\tan \delta$  with temperature are shown in Fig. 4.

As it could be observed, all nanocomposites presented the same viscoelastic pattern compared to that of the unfilled matrix. Indeed, a two modulus drop pattern was observed, related to the relaxation temperatures of the plasticizer-rich phase ( $T_{\alpha 1}$ ) and the starch-rich phase ( $T_{\alpha 2}$ ) [54]. In the case of  $T_{\alpha 1}$ , the relaxation temperature was not influenced by the incorporation of G and *Salvia* extracts and remains almost constant for high nanofiller contents. In contrast,  $T_{\alpha 2}$  was influenced by the G and *Salvia* extracts contents. Lower  $T_{\alpha 2}$  values were obtained for PLS – 1GE, whereas the value increased for PLS – 5GE samples. This fact suggested that G and *Salvia* extracts influenced the relaxation of the starch-rich phase, being the plasticizing effect of *Salvia* more remarkable at low G contents. However, as G content increased the reinforcing effect is more important over plasticizing effect and thus,  $T_{\alpha 2}$  tended to higher values. In addition, the incorporation of G nanoflakes

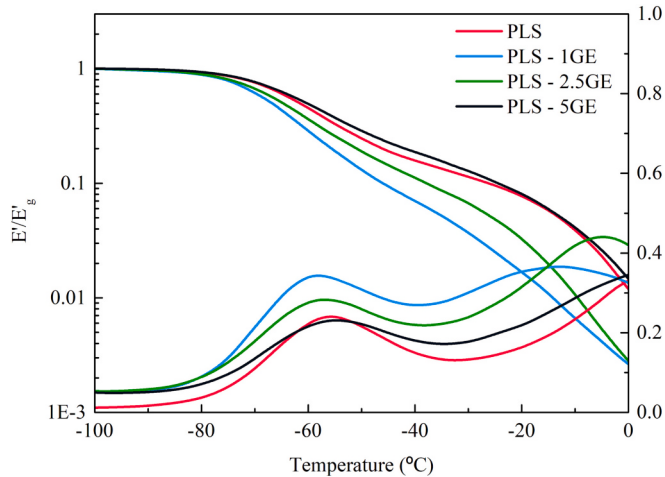


**Fig. 4.** Evolution of  $E'/E'_g$  and  $\tan \delta$  with temperature of PLS nanocomposite films reinforced with G.

and *Salvia* extracts led to a decrease of  $E'/E'_g$  for low contents, but the  $E'/E'_g$  increased after the addition of 5 wt% of G demonstrating the reinforcing behavior of G at high contents.

The mechanical behavior of nanocomposites reinforced with G was analyzed by means of tensile tests. The obtained results are presented in Table 1.

Results demonstrated that the addition of G nanoflakes resulted in higher Young's modulus, that moderately increased for 2.5 wt% of G and increased remarkably for a 5 wt% of G, achieving a value of 30.6 MPa for the highest G content. Regarding the strength behavior, a similar trend was observed, with no significant changes taking place for systems reinforced with 1 and 2.5 wt% of graphene, and with a remarkable increase being observed for the sample containing a 5 wt% of G. In contrast, it should be noted that there was a significant reduction of the elongation at break values with the addition of G, which, however, remained almost constant for all nanocomposites. The elongation decreased upon the addition of 1 wt% of G but remains constant for higher nanofiller contents. Thus, it was concluded that increasing the G

content, the stiffness and the strength of the material was progressively improved, while the flexibility was barely reduced. These results suggested that *Salvia* is acting as additional plasticizer and G as reinforcing agent and both effects are balanced.

Finally, in order to analyze the electrical response of PLS nanocomposites prepared with G, electrical conductivity measurements by two-probe technique were performed. In this sense, Abdo et al. demonstrated that electrically conductive nanocomposite films could be developed by the incorporation of conductive nanoparticles as G into polymeric matrices [4]. As it could be observed in Fig. 5a, the electrical conductivity of the nanocomposites increased with the G content compared to the non-conductive PLS matrix. However, it should be noted that the obtained electrical conductivity values were not as high as it would be desirable.

This little improvement could be due to two reasons. On one hand, the presence of *Salvia* extracts, as shown in Fig. 5b and c, can affect the arrangement of G nanoflakes, leading to holes and imperfections and thus, hindering the formation of an effective conductive network in the PLS nanocomposites. On the other hand, results could indicate that the conductive network was interrupted since graphene nanoflakes were embedded or ineffectively dispersed in the polymeric matrix.

These results are in agreement with those shown by Larraza et al. [42], who concluded that an efficient conductive network was not formed since G presented a damaged morphology, since *Salvia* extracts were attached to G nanoflakes, which in turn were embedded in the starch chains.

In order to further enhance reinforcement effect supplied by the nanoentities, graphene nanoflakes were replaced by graphene oxide nanoflakes, whose functional groups may be able to interact with the starch. Moreover, prepared nanocomposites were subsequently reduced to rGO, in order to supply them with electrical conductivity. In addition, this second proposed strategy allows the large-scale production of the material, since obtaining graphene oxide by Hummers' method requires shorter times compared to arduous graphene exfoliation resulting in a reduction of the energy consumption.

### 3.2. Effect of GO content on PLS nanocomposite films

Compared to G nanoflakes, GO showed much higher dispersibility in water thus facilitating the preparation of homogeneous films. Besides, the introduction of new oxidized functional groups would lead to better compatibility with the matrix, since strong nanofiller/matrix interactions could be formed. Thus, PLS nanocomposite films were prepared by adding different GO contents (1, 2.5 and 5 wt%) into the starch-based gelatinized matrix. However, it was expected that the resulting nanocomposites would not present electrical conductivity, as

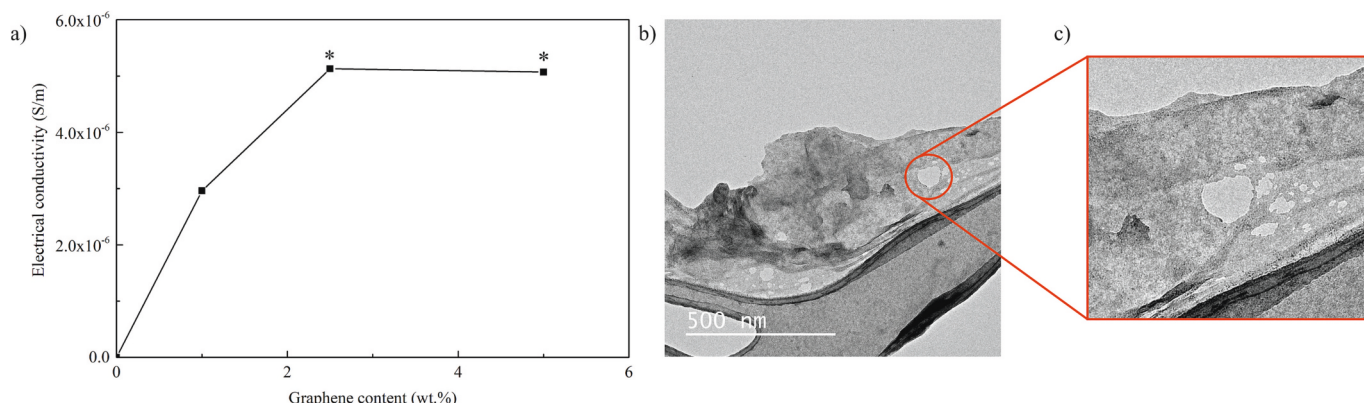


**Fig. 5.** a) Electrical conductivity against G content curves of PLS nanocomposite films reinforced with G, b) TEM image of G dispersed in water with *Salvia* extracts and c) amplified TEM image showing damaged morphology of G nanoflakes. Values analyzed using one-way ANOVA with Tukey's test, \* indicates statistical differences compared to the matrix, where  $p < 0.05$ .

GO in not electrically conductive [33].

The differences in the chemical structure of PLS and resulting nanocomposites reinforced with GO were investigated by FTIR measurements. Fig. 6 presented the obtained FTIR spectra of PLS and nanocomposite films.

In a similar way that occurred for PLS nanocomposites reinforced with G nanoflakes, the FTIR spectra of nanocomposites prepared adding GO showed some differences compared to the unfilled PLS matrix. As stated by other authors [47], after the incorporation of GO the bands at  $1650\text{ cm}^{-1}$ ,  $1150\text{ cm}^{-1}$  and  $1077\text{ cm}^{-1}$  shifted to lower wavenumber values due to the formation of H-bonds between starch chains and GO. In addition, the typical bands associated to the stretching vibrations of the C—O linkages in starch changed notably while increasing the GO content and, thus, while increasing the presence of new C—O linkages introduced with the oxidized nanofiller [55]. Finally, the appearance of a new peak related to GO and located near  $1740\text{ cm}^{-1}$ , mainly noticeable for the 5 wt% GO containing nanocomposite, is largely attributable to the presence of new carbonyl groups introduced in the oxidized graphene [47,56]. Besides, a band at  $1500\text{ cm}^{-1}$ , also observed in nanocomposites containing G, associated with C=C linkages in aromatic structure was observed [51].

The crystalline structure of nanocomposites reinforced with GO was analyzed by XRD. The resulting XRD patterns are shown in the Fig. 7. In addition to the broad peak at  $2\theta = 19.8^\circ$  related to residual starch crystallinity, all nanocomposites presented two new peaks associated with the presence of GO, namely at  $2\theta = 9.6^\circ$  and  $2\theta = 26.5^\circ$ , that were more intense as the nanofiller content increased. These signals are related to the (002) plane of GO and the residual pure graphitic structure, respectively [42,57]. However, it should be noted that in the case of nanocomposites the signal related to the (002) plane appeared shifted to lower values, i.e. from  $2\theta = 11.2^\circ$  for the neat GO [42] to  $2\theta = 9.6^\circ$ , indicating that the interlayer separation between GO nanoflakes increased from  $7.9\text{ \AA}$  for neat GO up to  $9.2\text{ \AA}$ , due to their incorporation into the PLS matrix and suggested effective interactions between starch chains and GO layers.

The wettability and surface properties of the nanocomposites reinforced with GO were also determined by contact angle analysis. The obtained measurements are presented in Table 2.

In contrast with the results obtained for nanocomposites reinforced with G and *Salvia* extracts, the addition of GO did not significantly affect the hydrophobicity of the films. Indeed, the nanocomposites showed contact angle values ranged from  $21.4^\circ$  to  $23.4^\circ$ , which were very close to that measured for the neat matrix. These results are in agreement with those reported by Grande et al. [14] that concluded that the wettability of the nanocomposites did not decrease after the incorporation of the GO.

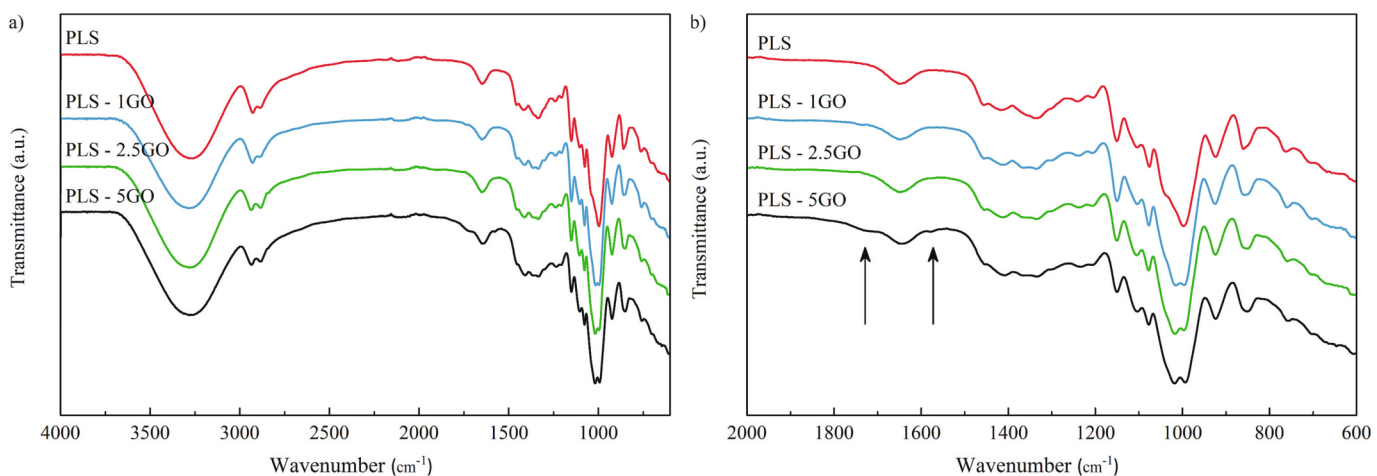


**Fig. 6.** FTIR spectra of PLS nanocomposite films reinforced with GO in the range of a) 4000–600  $\text{cm}^{-1}$  and b) a magnification in the range of 2000–600  $\text{cm}^{-1}$ .

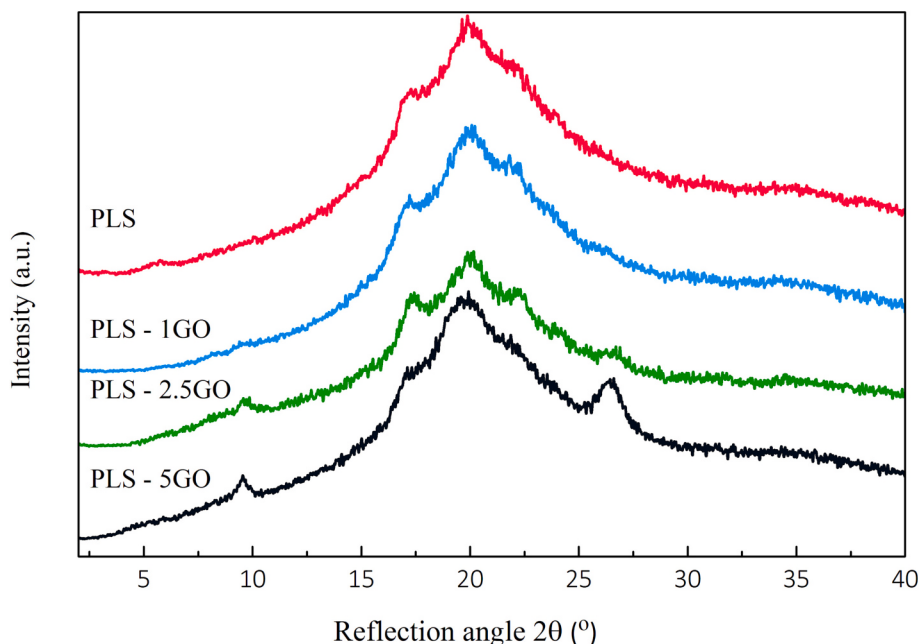


**Fig. 7.** XRD patterns of PLS nanocomposite films reinforced with GO.

**Table 2**

Contact angle measurements and mechanical properties of PLS – GO nanocomposite films. Values analyzed using one-way ANOVA with Tukey's test, \* indicates statistical differences compared to the matrix, where  $p < 0.05$ .

Sample	Contact angle (°)	Young's modulus (MPa)	Tensile strength (MPa)	Strain at break (%)
PLS	$24.6 \pm 0.3$	$7.9 \pm 0.9$	$1.4 \pm 0.1$	$57.9 \pm 0.5$
PLS – 1GO	$21.4 \pm 4.9$	$20.2 \pm 2.0 *$	$2.7 \pm 0.7 *$	$49.6 \pm 7.0$
PLS – 2.5GO	$21.4 \pm 1.4$	$21.7 \pm 1.9 *$	$2.6 \pm 0.1 *$	$29.5 \pm 5.3 *$
PLS – 5GO	$23.4 \pm 3.8$	$23.2 \pm 6.1 *$	$2.8 \pm 0.2 *$	$20.3 \pm 2.1 *$

The influence of the GO content in the viscoelastic behavior of PLS nanocomposite films was analyzed by DMA measurements. Fig. 8 presents the evolution of  $E'/E'_g$  and  $\tan \delta$  with temperature.

As noticed, the nanocomposite films reinforced with GO showed the same two-step modulus drop pattern of their counterparts containing G

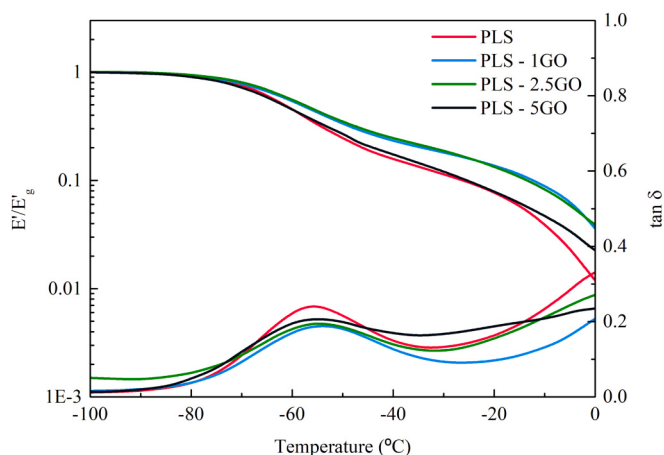


**Fig. 8.** Evolution of  $E'/E'_g$  and  $\tan \delta$  with temperature of PLS nanocomposite films reinforced with GO.

and *Salvia* extracts.  $T_{\alpha 1}$  remained constant after the incorporation of GO, however  $T_{\alpha 2}$  shifted to higher temperatures for PLS – 1GO and PLS – 2.5GO and widened for PLS – 5GO. This change indicated that GO at 1 and 2.5 wt% reduced the mobility of starch-rich phase, which could be due to effective formation of hydrogen bonding interactions between the oxygen containing functional groups of GO and starch. Both relaxation magnitudes decreased due to the decrease of the amount of glycerol molecules and starch chains relaxed at these transitions.

Tensile test measurements were performed to determine the influence of GO content in the mechanical properties of PLS nanocomposites. The obtained results are shown in Table 2.

As it could be observed the nanocomposites reinforced with GO presented significantly higher Young's modulus and tensile strength values than the PLS matrix, whereas lower elongation at break values were obtained. As stated by Li et al. [47], the incorporation of GO improved the strength and the stiffness of starch-based materials due to the good dispersion of the nanofiller in the matrix and the strong PLS/GO interactions. Compared to nanocomposites reinforced with G, it should be mentioned that higher tensile values were obtained due to the ability of oxygen containing groups of GO to interact with starch. However, lower elongation at break values were obtained since as mentioned above, *Salvia* extracts could be behaving as plasticizers in nanocomposites with G.

Regarding the electrical conductivity measurements, GO reinforced nanocomposites did not show electrical conductivity. As defined by other authors, GO is electrically non-conductive [49,50,58] since during the oxidation reaction the electronic structure of graphite is disrupted due to the destruction of  $\pi$ -conjugation [49]. As neither of the GO containing films showed an electrical conductive character, and taking into account the will to supply electrical conductivity to the starch-based materials, the prepared films were reduced using ascorbic acid as reducing agent. As has been reported in literature [50], after a reduction process the hexagonal lattice could be expected to be restored leading to conductive materials. However, the GO is not usually completely

reduced, and the residual hydroxyl, epoxide, carbonyl and carboxyl groups that remains intact could continue contributing to the formation of rGO/starch interactions [50].

First, the success of the employed method to reduce the GO nanoflakes was demonstrated by means of XRD and contact angle measurements.

The diffractograms of reduced films are presented in Fig. 9. As it was detected for the GO containing nanocomposites, a broad peak centered around  $2\theta = 19.8^\circ$  was observed, and a peak around  $2\theta = 26.5^\circ$ , associated to PLS residual crystallinity and the (002) plane of hexagonal structure of pristine graphite [59–61]. Besides, the characteristic peak of GO located at  $2\theta = 9.6^\circ$  disappeared after the reduction, revealing that the oxygenated groups were successfully removed [62].

As the chemical reduction with ascorbic acid could eliminate the hydroxyl, epoxide and carbonyl groups in the structure of GO, the wettability of the nanocomposites is expected to be reduced. Thus, in order to analyze the success of the reduction with ascorbic acid on the surface properties, contact angle measurements were performed.

As it could be noted, the wettability of the PLS films decreased after the reduction reaction, obtaining higher angle values for reduced nanocomposite materials. The measured contact angle value was significantly increased from  $24.6 \pm 0.3^\circ$  for the unfilled matrix to  $35.5 \pm 2.2^\circ$  and  $46.5 \pm 1.5^\circ$  for PLS – 2.5rGO and PLS – 5rGO nanocomposites, subsequently. Similar results were published by Romani et al. for polyurethane composites reinforced with rGO [63]. Therefore, it was concluded that the hydrophobicity of the films was improved since the oxygen groups were satisfactorily removed.

The results are in concordance with those conclusions obtained by XRD, demonstrating that during the reduction reaction the oxygen functional groups of GO were almost fully eliminated and, thus, it was concluded that the employed reaction conditions were successful.

As published elsewhere the reduction of GO restores the  $sp^2$  hybridized structure of the G [50] leading to electrically conductive nanoflakes [62]. Thus, once the success of the chemical reduction of GO

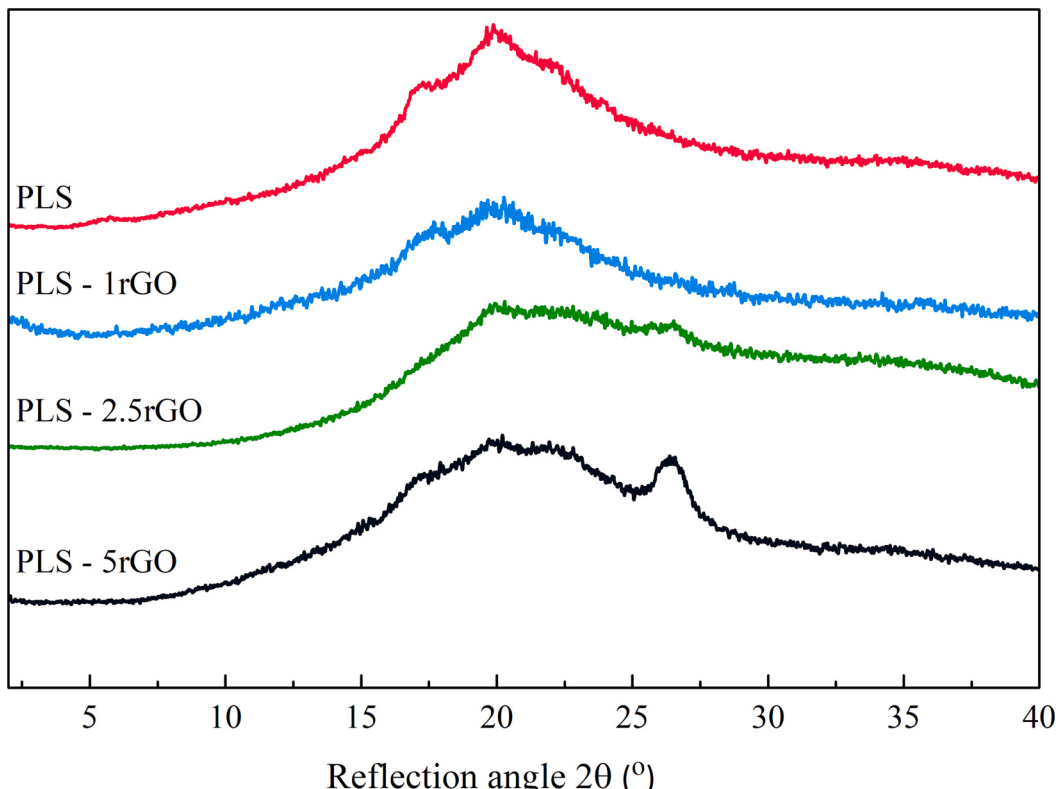


Fig. 9. XRD patterns of PLS nanocomposite films reinforced with rGO.

was demonstrated, the influence of the reaction in the electrical behavior of PLS nanocomposites was evaluated. The electrical conductivity results are shown in Fig. 10.

In contrast with GO containing nanocomposites, all reduced films showed electrical conductivity, increasing for higher rGO contents. Besides, comparing the nanocomposites reinforced with rGO to those prepared using G, the higher conductivity values achieved for the former may be due to two reasons: 1) a more uniform initial dispersion of GO into the matrix and GO/interactions which resulted in the formation of a more effective conductive network once reduced, 2) the *Salvia* used to stabilize G suspension in water and incorporated to the gelatinized starch, could hinder the formation of a conductive network, as previously discussed. These conclusions would also be supported by the mechanical properties of GO containing films. Hence, higher tensile strength values were obtained for GO containing samples indicating good stress transfer from the matrix to the GO. In addition, higher elongation at break values were obtained for samples reinforced with G suggesting that *Salvia* acts as plasticizer of starch. Thus, it was concluded that the use of ascorbic acid as reducing agent to restore the electronic structure of GO was suitable.

In order to corroborate the electrically conductive results obtained by semiconductor analysis and willing to compare the electric behavior of the different systems, conductive properties of the films were also analyzed by EFM measurements. In this case, for comparative reasons, samples containing the highest reinforcement content, i.e. 5 wt% of GE, GO or rGO, were selected to be analyzed. Obtained images are collected in Fig. 11. As defined in literature [42,43], when a voltage is applied through the sample, only conductor areas are capable of interacting with the cantilever leading to bright phase EFM images, allowing to distinguish between insulating and conductive samples.

As expected, the plasticized starch matrix did not produce any bright areas since no electrical response was generated, due to its non-conductive character. On the other hand, some slightly bright regions could be distinguished for PLS-5GE sample, signaling to a limited but existing electrically conductive capacity. However, bright spots observed for this system were sparse and isolated, which could be due to a not continuous conductive network being formed, as previously signaled by two-probe electrical tests. The electrical response for PLS-5GO film was almost null, which is to be expected due to the non-electrical character of graphene oxide. In contrast, a remarkably

electrically conductive surface was observed for PLS-5rGO film, with EFM images showing extremely bright images compared to all other systems, corroborating the better electrically conductivity behavior of the latter sample. Thus, in agreement with previous results, it could be concluded that the use of reduced graphene oxide is the most effective alternative to prepare starch-based electrically conductive materials.

With the aim of verifying differences in the dispersibility of each reinforcement and evaluate its effect of final properties of the obtained materials, the morphology of the unfilled matrix and the resulting nanocomposite films was analyzed by SEM. Recorded micrographs are presented in Fig. 12. As it could be observed, the unfilled PLS matrix showed a relatively smooth morphology (Fig. 12a). Similarly, films containing GO nanoflakes exhibited a similar homogeneous morphology compared to the matrix, maintained also after the reduction with ascorbic acid, indicating that in those cases the reinforcement was effectively incorporated. In contrast, significant differences were observed after the addition of G nanoflakes and *Salvia* extract. As noticed in Fig. 12b, G nanoflakes are randomly embedded in the PLS matrix, suggesting the presence of G agglomerates. As concluded by Ashori, high G contents could easily result in aggregates of graphene nanosheets in the PLS matrix [64]. These results corroborated that the good dispersion of GO and rGO in the matrix, as well as the strong filler/polymer interactions, resulted in a remarkable improvement of the mechanical properties and electrical conductivity, while the presence of G agglomerates in the matrix led to an inefficient reinforcement effect while hindering the formation of a conductive network.

#### 4. Conclusions

PLS nanocomposite films were successfully obtained by the incorporation of carbonaceous nanoparticles, i.e. G and GO. In addition, the nanocomposites prepared with GO were reduced in order to achieve better electrical conductivity properties.

Firstly, G containing nanocomposites were prepared using different nanofiller contents. *Salvia* extracts were necessarily incorporated in order to facilitate the dispersion of G in the aqueous gelatinization media. The influence of adding different G contents into the matrix was analyzed. It was demonstrated that the addition of G nanoflakes slightly increased the hydrophobicity character. Just the incorporation of 1 wt% of GE resulted in an increase of the contact angle up to 37.2°. In contrast,

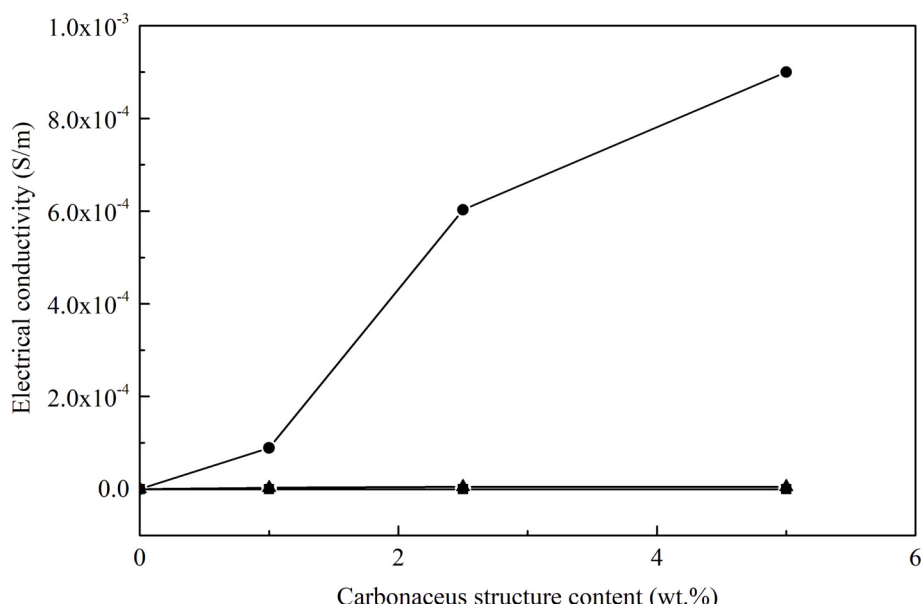


**Fig. 10.** Electrical conductivity against carbonaceous structure content curves of PLS nanocomposite films reinforced with G and extracts (▲), GO (■) and rGO (●). Values analyzed using one-way ANOVA with Tukey's test, \* indicates statistical differences compared to the matrix, where  $p < 0.05$ .

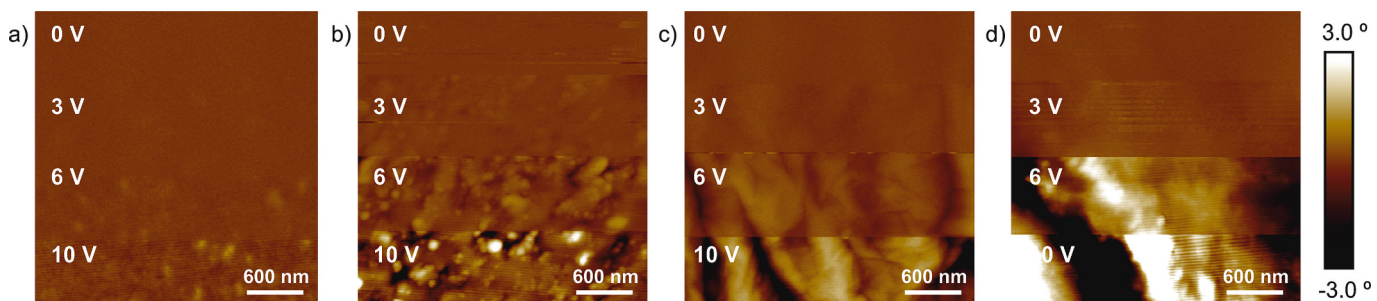


**Fig. 11.** EFM phase images at 0, 3, 6 and 10 V for a) PLS, b) PLS-5GE, c) PLS-5GO and d) PLS-5rGO (Image size: 3 × 3 μm).

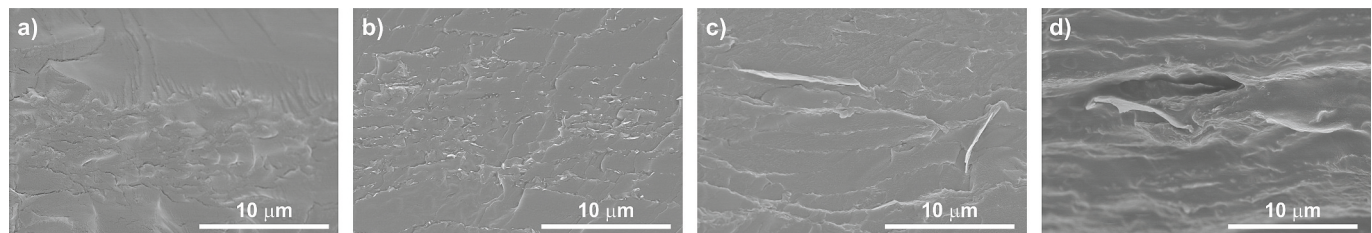


**Fig. 12.** SEM images of transversal section of a) PLS, b) PLS-5GE, c) PLS-5GO and d) PLS-5rGO nanocomposite films.

some plasticizing effect of *Salvia* could be concluded. Besides, as expected the mechanical properties were improved compared to the unfilled matrix. Both the Young's modulus and the tensile strength values were significantly increased for the highest G content, achieving values of 30.6 MPa and 2.2 MPa, subsequently. However, the electrical conductivity was affected by the presence of *Salvia* extracts.

On the other hand, in a similar way, PLS nanocomposites were developed adding GO as nanofiller. Regarding the results, as hypothesized the strong starch/GO interactions and the good dispersion of GO improved the final behavior of the films, specially the mechanical properties. Besides, these films were satisfactorily reduced by heating them in presence of ascorbic acid. As considered, the  $sp^2$  hybridized structure of GO was restored, obtaining electrical conductivity values of  $9.0 \times 10^{-4}$  S/m for the highest rGO content.

Supplementary data to this article can be found online at <https://doi.org/10.1016/j.ijbiomac.2023.126130>.

#### CRediT authorship contribution statement

**Kizkitza González:** Methodology, Investigation, Writing – original draft. **Izaskun Larraza:** Investigation, Writing – original draft. **Loli Martin:** Methodology, Investigation. **Arantxa Eceiza:** Supervision. **Nagore Gabilondo:** Conceptualization, Writing – review & editing, Supervision.

#### Declaration of competing interest

The authors declare that they have no known competing financial interests or personal relationships that could have appeared to influence the work reported in this paper.

#### Data availability

The data will be made available on request.

#### Acknowledgments

Authors thank the financial support from the University of the Basque Country (UPV/EHU) (GIU18/216 Research Group), from the Basque Government in the frame of Elkartek KK-2020/00053 and PIBA2020-1

0041 and from Spanish Ministry of Science, Innovation and Universities and European Union (MICINN/EU/FEDER) in the frame of PID2019-105090RB-I00 projects, are gratefully acknowledged. Moreover, we are grateful to the Macrobehavior-Mesostructure-Nanotechnology SGiker unit of the UPV/EHU. K. González thanks the University of the Basque Country for the PhD grant (PIF-G-003-2015) and the grant “Contratación de doctores recientes hasta su integración en programas de formación postdoctoral en la UPV/EHU «DOKBERRI» 2020-I” (DOCREC20/07).

#### References

- [1] K. Li, S. Jin, X. Li, S.Q. Shi, J. Li, A green bio-inspired chelating design for improving the electrical conductivity of flexible biopolymer-based composites, *J. Clean. Prod.* 285 (2021), 125504, <https://doi.org/10.1016/j.jclepro.2020.125504>.
- [2] X. Zhang, Y. Tang, F. Zhang, C.S. Lee, A novel aluminum–graphite dual-ion battery, *Adv. Energy Mater.* 6 (2016) 1–6, <https://doi.org/10.1002/aenm.201502588>.
- [3] Z. Sun, T. Wang, R. Zhang, H. Li, Y. Wu, S. Toan, Z. Sun, Boosting hydrogen production via deoxygenation-sorption-enhanced biomass gasification, *Bioresour. Technol.* 382 (2023), <https://doi.org/10.1016/j.biortech.2023.129197>.
- [4] H.S. Abdo, A.A. Elzatahy, H.F. Alharbi, K.A. Khalil, Electrical Conductivity Behavior of Biopolymer Composites, Elsevier Inc., 2017, <https://doi.org/10.1016/B978-0-12-809261-3.00002-4>.
- [5] Z. Huang, P. Luo, H. Zheng, Z. Lyu, X. Ma, Novel one-dimensional V3S4@NC nanofibers for sodium-ion batteries, *J. Phys. Chem. Solids* 172 (2023), 111081, <https://doi.org/10.1016/j.jpcs.2022.111081>.
- [6] Z. Wang, W. Fu, L. Hu, M. Zhao, T. Guo, D. Hrynsphan, S. Tatsiana, J. Chen, Improvement of electron transfer efficiency during denitrification process by Fe-Pd/multi-walled carbon nanotubes: possessed redox characteristics and secreted endogenous electron mediator, *Sci. Total Environ.* 781 (2021), 146686, <https://doi.org/10.1016/j.scitotenv.2021.146686>.
- [7] Z. Wang, L. Dai, J. Yao, T. Guo, D. Hrynsphan, S. Tatsiana, J. Chen, Enhanced adsorption and reduction performance of nitrate by Fe-Pd-Fe3O4 embedded multi-walled carbon nanotubes, *Chemosphere.* 281 (2021), 130718, <https://doi.org/10.1016/j.chemosphere.2021.130718>.
- [8] G. Huang, Q. Kong, W. Yao, Q. Wang, High proportion of active nitrogen-doped hard carbon based on Mannich reaction as anode material for high-performance sodium-ion batteries, *ChemSusChem.* 16 (2023), <https://doi.org/10.1002/cssc.202202070>.
- [9] K.M. Dang, R. Yoksan, E. Pollet, L. Avérous, Morphology and properties of thermoplastic starch blended with biodegradable polyester and filled with halloysite nanoclay, *Carbohydr. Polym.* 242 (2020), 116392, <https://doi.org/10.1016/j.carbpol.2020.116392>.
- [10] N. Follain, J. Ren, E. Pollet, L. Avérous, Study of the water sorption and barrier performances of potato starch nano-biocomposites based on halloysite nanotubes, *Carbohydr. Polym.* 277 (2022), <https://doi.org/10.1016/j.carbpol.2021.118805>.

- [11] A. Apriyanto, J. Compart, J. Fettke, A review of starch, a unique biopolymer – structure, metabolism and in planta modifications, *Plant Sci.* 318 (2022), 111223, <https://doi.org/10.1016/j.plantsci.2022.111223>.
- [12] M. Azizi-Lalabadi, S.M. Jafari, Bio-nanocomposites of graphene with biopolymers; fabrication, properties, and applications, *Adv. Colloid Interf. Sci.* 292 (2021), 102416, <https://doi.org/10.1016/j.cis.2021.102416>.
- [13] K. González, L. Iturriaga, A. González, A. Eceiza, N. Gabilondo, Improving mechanical and barrier properties of thermoplastic starch and polysaccharide nanocrystals nanocomposites, *Eur. Polym. J.* 123 (2020), 109415, <https://doi.org/10.1016/j.eurpolymj.2019.109415>.
- [14] C.D. Grande, J. Mangadlao, J. Fan, A. De Leon, J. Delgado-Ospina, J.G. Rojas, D. F. Rodrigues, R. Advincula, Chitosan cross-linked graphene oxide nanocomposite films with antimicrobial activity for application in food industry, *Macromol. Symp.* 374 (2017) 1–8, <https://doi.org/10.1002/masy.201600114>.
- [15] H. Ji, H. Sun, X. Qu, Antibacterial applications of graphene-based nanomaterials: recent achievements and challenges, *Adv. Drug Deliv. Rev.* 105 (2016) 176–189, <https://doi.org/10.1016/j.addr.2016.04.009>.
- [16] S. Ganguly, D. Ray, P. Das, P.P. Maity, S. Mondal, V.K. Aswal, S. Dhara, N.C. Das, Mechanically robust dual responsive water dispersible-graphene based conductive elastomeric hydrogel for tunable pulsatile drug release, *Ultrason. Sonochem.* 42 (2018) 212–227, <https://doi.org/10.1016/j.ulsonch.2017.11.028>.
- [17] L. Sha, B. Bin Sui, P. Fei Wang, Z. Gong, Y. Hang Zhang, Y. Han Wu, L. Na Zhao, F. Nian Shi, Printing 3D mesh-like grooves on zinc surface to enhance the stability of aqueous zinc ion batteries, *J. Colloid Interface Sci.* 647 (2023) 421–428, <https://doi.org/10.1016/j.jcis.2023.05.171>.
- [18] K. González, C. García-Astrain, A. Santamaría-Echart, L. Ugarte, L. Avérous, A. Eceiza, N. Gabilondo, Starch/graphene hydrogels via click chemistry with relevant electrical and antibacterial properties, *Carbohydr. Polym.* 202 (2018) 372–381, <https://doi.org/10.1016/j.carbpol.2018.09.007>.
- [19] S. Vandghanooni, M. Eskandani, Electrically conductive biomaterials based on natural polysaccharides: challenges and applications in tissue engineering, *Int. J. Biol. Macromol.* 141 (2019) 636–662, <https://doi.org/10.1016/j.ijbiomac.2019.09.020>.
- [20] A. Mohamed, T. Ardyani, S. Abu Bakar, M. Sagisaka, Y. Umetsu, J.J. Hamon, B. A. Rahim, S.R. Esa, H.P.S. Abdul Khalil, M.H. Mamat, S. King, J. Eastoe, Rational design of aromatic surfactants for graphene/natural rubber latex nanocomposites with enhanced electrical conductivity, *J. Colloid Interface Sci.* 516 (2018) 34–47, <https://doi.org/10.1016/j.jcis.2018.01.041>.
- [21] A. Santamaría-Echart, I. Fernandes, F. Barreiro, A. Retegi, A. Arbelaitz, M. A. Corcueria, A. Eceiza, Development of waterborne polyurethane-ureas added with plant extracts: study of different incorporation routes and their influence on particle size, thermal, mechanical and antibacterial properties, *Prog. Org. Coatings.* 117 (2018) 76–90, <https://doi.org/10.1016/j.porgcoat.2018.01.006>.
- [22] Y. Liu, Y. Li, X. Yuan, R. Ren, Y. Lv, A self-prepared graphene oxide/sodium alginate aerogel as biological carrier to improve the performance of a heterotrophic nitrifier, *Biochem. Eng. J.* 171 (2021), 108027, <https://doi.org/10.1016/j.bej.2021.108027>.
- [23] F. Han Lyn, C.P. Tan, R.M. Zawawi, Z.A. Nur Hanani, Enhancing the mechanical and barrier properties of chitosan/graphene oxide composite films using trisodium citrate and sodium tripolyphosphate crosslinkers, *J. Appl. Polym. Sci.* 138 (2021) 1–14, <https://doi.org/10.1002/app.50618>.
- [24] D. Kaya, N. Alemdar, Electroconductive hyaluronic acid/gelatin/poly(ethylene oxide) polymeric film reinforced by reduced graphene oxide, *J. Appl. Polym. Sci.* 136 (2019) 31–34, <https://doi.org/10.1002/app.46905>.
- [25] Z. Ding, Y. Tang, P. Zhu, Reduced graphene oxide/cellulose nanocrystal composite films with high specific capacitance and tensile strength, *Int. J. Biol. Macromol.* 200 (2022) 574–582, <https://doi.org/10.1016/j.ijbiomac.2022.01.130>.
- [26] L. Zhang, L. Xu, Y. Wang, J. Liu, G. Tan, F. Huang, N. He, Z. Lu, A novel therapeutic vaccine based on graphene oxide nanocomposite for tumor immunotherapy, *Chinese Chem. Lett.* 33 (2022) 4089–4095, <https://doi.org/10.1016/j.cclet.2022.01.071>.
- [27] D.S. Shin, H.G. Kim, H.S. Ahn, H.Y. Jeong, Y.J. Kim, D. Odkhuu, N. Tsogbadrakh, H.B.R. Lee, B.H. Kim, Distribution of oxygen functional groups of graphene oxide obtained from low-temperature atomic layer deposition of titanium oxide, *RSC Adv.* 7 (2017) 13979–13984, <https://doi.org/10.1039/c7ra00114b>.
- [28] A. Jiríčková, O. Jankovský, Z. Sofer, D. Sedmidubský, Synthesis and applications of graphene oxide, *Materials (Basel)*, 15 (2022), <https://doi.org/10.3390/ma15030920>.
- [29] Y. Ma, Y. Leng, D. Huo, D. Zhao, J. Zheng, H. Yang, P. Zhao, F. Li, C. Hou, A sensitive enzyme-free electrochemical sensor based on a rod-shaped bimetallic MOF anchored on graphene oxide nanosheets for determination of glucose in huangshui, *Anal. Methods* 15 (2023) 2417–2426, <https://doi.org/10.1039/d2ay01977a>.
- [30] A. Usman, Z. Hussain, A. Riaz, A.N. Khan, Enhanced mechanical, thermal and antimicrobial properties of poly(vinyl alcohol)/graphene oxide/starch/silver nanocomposites films, *Carbohydr. Polym.* 153 (2016) 592–599, <https://doi.org/10.1016/j.carbpol.2016.08.026>.
- [31] M.R. Islam, S.I. Mollik, Enhanced electrochemical performance of flexible and eco-friendly starch/graphene oxide nanocomposite, *Heliyon*. 6 (2020), <https://doi.org/10.1016/j.heliyon.2020.e05292>.
- [32] S. Afshar, H. Baniasadi, Investigation the effect of graphene oxide and gelatin/starch weight ratio on the properties of starch/gelatin/GO nanocomposite films: the RSM study, *Int. J. Biol. Macromol.* 109 (2018) 1019–1028, <https://doi.org/10.1016/j.ijbiomac.2017.11.083>.
- [33] M.F. Zainuddin, N.H. Nik Raikhan, N.H. Othman, W.F.H. Abdullah, Synthesis of reduced graphene oxide (rGO) using different treatments of graphene oxide (GO), *IOP Conf. Ser. Mater. Sci. Eng.* 358 (2018), <https://doi.org/10.1088/1757-899X/358/1/012046>.
- [34] A. Razaq, F. Bibi, X. Zheng, R. Papadakis, S.H.M. Jafri, H. Li, Review on graphene-, graphene oxide-, reduced graphene oxide-based flexible composites: from fabrication to applications, *Materials (Basel)*, 15 (2022), <https://doi.org/10.3390/ma15031012>.
- [35] D. Shahdeo, A. Roberts, N. Abbidene, S. Gandhi, Graphene based sensors, *Compr. Anal. Chem.* (2020) 175–199.
- [36] L. Liang, Z. Li, Z. Bai, Y. Feng, X. Guo, J. Ma, C. Liu, Dependence of electromagnetic wave absorption properties on the topography of Ni anchoring on reduced graphene oxide, *Chinese Chem. Lett.* 32 (2021) 870–874, <https://doi.org/10.1016/j.cclet.2020.06.014>.
- [37] C. Hao, T. Gao, A. Yuan, J. Xu, Synthesis of iron oxide cubes/reduced graphene oxide composite and its enhanced lithium storage performance, *Chinese Chem. Lett.* 32 (2021) 113–118, <https://doi.org/10.1016/j.cclet.2020.11.038>.
- [38] X.G. Gao, L.X. Cheng, W.S. Jiang, X.K. Li, F. Xing, Graphene and its derivatives-based optical sensors, *Front. Chem.* 9 (2021) 1–13, <https://doi.org/10.3389/fchem.2021.615164>.
- [39] A.P.G. Carvalho, E.C.B.A. Alegria, A. Fantoni, A.M. Ferraria, M. Ana, B. Rego, A.P. C. Ribeiro, Effect of graphene vs. reduced graphene oxide in gold nanopartiles for optical biosensors — a comparative study, *Biosensors*, 12 (2022) 163–182.
- [40] D. Bu, Y. Zhou, C. Yang, H. Feng, C. Cheng, M. Zhang, Z. Xu, L. Xiao, Y. Liu, Z. Jin, Preparation of quaternarized N-halamine-grafted graphene oxide nanocomposites and synergistic antibacterial properties, *Chinese Chem. Lett.* 32 (2021) 3509–3513, <https://doi.org/10.1016/j.cclet.2021.03.007>.
- [41] M. Kurian, Recent progress in the chemical reduction of graphene oxide by green reductants – A Mini review, *Carbon Trends*, 5 (2021), 100120, <https://doi.org/10.1016/j.cartre.2021.100120>.
- [42] I. Larraza, B. Alonso-Lerma, K. Gonzalez, N. Gabilondo, R. Perez-Jimenez, M. A. Corcueria, A. Arbelaitz, A. Eceiza, Waterborne polyurethane and graphene/graphene oxide-based nanocomposites: reinforcement and electrical conductivity, *Express Polym Lett* 14 (2020) 1018–1033, <https://doi.org/10.3144/expresspolymllett.2020.83>.
- [43] L. Ugarte, S. Gómez-Fernández, A. Tercjak, A. Martínez-Amesti, M.A. Corcueria, A. Eceiza, Strain sensitive conductive polyurethane foam/graphene nanocomposites prepared by impregnation method, *Eur. Polym. J.* 90 (2017) 323–333, <https://doi.org/10.1016/j.eurpolymj.2017.03.035>.
- [44] N.L. García, L. Ribba, A. Dufresne, M.I. Aranguren, S. Goyanes, Physico-mechanical properties of biodegradable starch nanocomposites, *Macromol. Mater. Eng.* 294 (2009) 169–177, <https://doi.org/10.1002/mame.200800271>.
- [45] B. Alonso-Lerma, L. Barandiaran, L. Ugarte, I. Larraza, A. Reifs, R. Olmos-Juste, N. Barruetabénia, I. Amenabar, R. Hillenbrand, A. Eceiza, R. Perez-Jimenez, High performance crystalline nanocellulose using an ancestral endoglucanase, *Commun. Mater.* 1 (2020), <https://doi.org/10.1038/s43246-020-00055-5>.
- [46] W.L. Bragg, The dawn of X-ray crystallography, *Proc. Camb. Philol. Soc.* 12 (1913) 43–57.
- [47] R. Li, C. Liu, J. Ma, Studies on the properties of graphene oxide-reinforced starch biocomposites, *Carbohydr. Polym.* 84 (2011) 631–637, <https://doi.org/10.1016/j.carbpol.2010.12.041>.
- [48] J.-L. Li, M. Zhou, G. Cheng, F. Cheng, Y. Lin, P.-X. Zhu, Comparison of mechanical reinforcement effects of cellulose nanofibers and montmorillonite in starch composite, *Starch - Stärke*. 1800114 (2018) 1–9, <https://doi.org/10.1002/star.201800114>.
- [49] T.B. Rouf, J.L. Kokini, Biodegradable biopolymer-graphene nanocomposites, *J. Mater. Sci.* 51 (2016) 9915–9945, <https://doi.org/10.1007/s10853-016-0238-4>.
- [50] T. Ma, P.R. Chang, P. Zheng, X. Ma, The composites based on plasticized starch and graphene oxide/reduced graphene oxide, *Carbohydr. Polym.* 94 (2013) 63–70, <https://doi.org/10.1016/j.carbpol.2013.01.007>.
- [51] J. Li, M. Zhou, G. Cheng, F. Cheng, Y. Lin, P.X. Zhu, Fabrication and characterization of starch-based nanocomposites reinforced with montmorillonite and cellulose nanofibers, *Carbohydr. Polym.* 210 (2019) 429–436, <https://doi.org/10.1016/j.carbpol.2019.01.051>.
- [52] K. González, L. Martin, A. Retegi, A. Eceiza, N. Gabilondo, D-isosorbide and 1,3-propanediol as plasticizers for starch-based films: characterization and aging study, *J. Appl. Polym. Sci.* 134 (2017) 1–10, <https://doi.org/10.1002/app.44793>.
- [53] X. Gong, G. Liu, Y. Li, D.Y.W. Yu, W.Y. Teoh, Functionalized-graphene composites: fabrication and applications in sustainable energy and environment, *Chem. Mater.* 28 (2016) 8082–8118, <https://doi.org/10.1021/acs.chemmater.6b01447>.
- [54] K. González, A. Retegi, A. González, A. Eceiza, N. Gabilondo, Starch and cellulose nanocrystals together into thermoplastic starch bionanocomposites, *Carnohydro Polym.* 117 (2015) 83–90, <https://doi.org/10.1016/j.carbpol.2014.09.055>.
- [55] P. Zheng, T. Ma, X. Ma, Fabrication and properties of starch-grafted graphene nanosheet/ plasticized-starch composites, *Ind. Eng. Chem. Res.* 52 (2013) 14201–14207, <https://doi.org/10.1021/ie402220d>.
- [56] C. Geng, F. Zhao, H. Niu, J. Zhang, H. Dong, Z. Li, H. Chen, Enhancing the permeability, anti-biofouling performance and long-term stability of TFC nanofiltration membrane by imidazole-modified carboxylated graphene oxide/polyethersulfone substrate, *J. Membr. Sci.* 664 (2022), 121099, <https://doi.org/10.1016/j.memsci.2022.121099>.
- [57] J. Guerrero-Contreras, F. Caballero-Briones, Graphene oxide powders with different oxidation degree, prepared by synthesis variations of the hummers method, *Mater. Chem. Phys.* 153 (2015) 209–220, <https://doi.org/10.1016/j.matchemphys.2015.01.005>.

- [58] P.K.S. Mural, M. Sharma, G. Madras, S. Bose, A critical review on *in situ* reduction of graphene oxide during preparation of conducting polymeric nanocomposites, RSC Adv. 5 (2015) 32078–32087, <https://doi.org/10.1039/c5ra02877a>.
- [59] J. Fan, Z. Shi, J. Wang, J. Yin, Glycidyl methacrylate-modified gum arabic mediated graphene exfoliation and its use for enhancing mechanical performance of hydrogel, Polymer (Guildf). 54 (2013) 3921–3930, <https://doi.org/10.1016/j.polymer.2013.05.057>.
- [60] J. Cao, Y. Zhu, X. Yang, Y. Chen, Y. Li, H. Xiao, W. Hou, J. Liu, The promising photo anode of graphene/zinc titanium mixed metal oxides for the CdS quantum dot-sensitized solar cell, Sol. Energy Mater. Sol. Cells 157 (2016) 814–819, <https://doi.org/10.1016/j.solmat.2016.08.003>.
- [61] E. Mahmoudi, L.Y. Ng, M.M. Ba-Abbad, A.W. Mohammad, Novel nanohybrid polysulfone membrane embedded with silver nanoparticles on graphene oxide nanoplates, Chem. Eng. J. 277 (2015) 1–10, <https://doi.org/10.1016/j.cej.2015.04.107>.
- [62] I. Kanayama, H. Miyaji, H. Takita, E. Nishida, M. Tsuji, B. Fugetsu, L. Sun, K. Inoue, A. Ibara, T. Akasaka, T. Sugaya, M. Kawanami, Comparative study of bioactivity of collagen scaffolds coated with graphene oxide and reduced graphene oxide, Int. J. Nanomedicine 9 (2014) 3363–3373, <https://doi.org/10.2147/IJN.S62342>.
- [63] E.C. Romani, S. Nardeccchia, C. Vilani, S. Qi, H. Dong, F.L. Freire, Synthesis and characterization of polyurethane/reduced graphene oxide composite deposited on steel, J. Coatings Technol. Res. 15 (2018) 1371–1377, <https://doi.org/10.1007/s11998-018-0088-x>.
- [64] Alireza Ashori, Effects of graphene on the behavior of chitosan and starch nanocomposite films, Polym. Eng. Sci. 54 (2014) 2215–2460, <https://doi.org/10.1002/pen>.